XVIII IMEKO WORLD CONGRESS
Metrology for a Sustainable Development
September, 17-22, 2006, Rio de Janeiro, Brazil

MAGNETORESISTIVE BIOSENSOR MODELLING FOR BIOMOLECULAR RECOGNITION

T. M. Almeida[1], *M. S. Piedade*[1], *P. C. Lopes*[1], *L. Sousa*[1], *J. Germano*[1], *F. Cardoso*[2], *H. A. Ferreira*[2], *P. P. Freitas*[2]

[1] INESC-ID/IST, Lisboa, Portugal
{ Teresa.Almeida@inesc-id.pt, msp@inesc-id.pt, Paulo.C.Lopes@inesc-id.pt, Leonel.Sousa@inesc-id.pt, jahg@sips.inesc-id.pt }

[2] INESC-MN/IST, Lisboa, Portugal
{ fcardoso@inesc-mn.pt, hferreira@inesc-mn.pt, pfreitas@inesc-mn.pt }

Abstract: This paper presents the modelling of a magnetic biosensor included on a hand held microsystem based on a fully integrated magnetoresistive biochip for biomolecular recognition (DNA hybridisation, antibody antigen interaction, etc.) [1]. The biochip uses magnetic field arraying of magnetically tagged biomolecules and high sensitivity sensors which can be used to detect single or few biomolecules. The biosensor has an matrix-array structure and each biosensor site consists of a thin film diode in series with a magnetic tunnel junction. Schottky and *pin* diodes are used as temperature sensors and switching devices, although this paper specially emphasises *pin* diodes characterisation. A complete theoretical model characterising biosensor electrical, temperature and magnetic behaviour is derived and experimental results are provided.

Keywords: biosensor modelling, biochip, magnetoresistive sensor, biomolecular recognition.

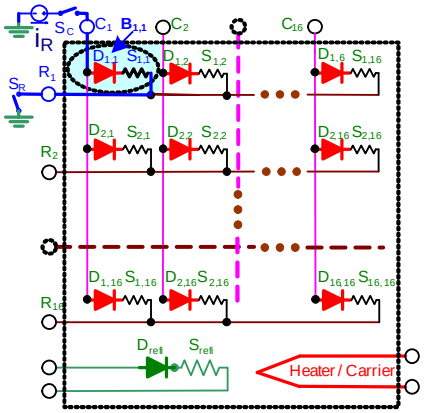

Figure 1: Magnetoresistive biochip simplified electrical scheme.

1. INTRODUCTION

Recently, magnetoresistive biochips have been introduced for fully integrated biomolecular recognition assays, using target biomolecules marked with magnetic particles. Among the various types of magnetic sensors, magnetic tunnel junctions (MTJ) assume greater importance because of their greater flexibility in resistance design and because they benefit from recent research and technological advances aiming the design of future ultra high density magnetic memory chips and higher magnetic sensitivity, when compared with other types of magnetic sensors, which enables the detection of smaller magnetic labels [2, 3].

A compact (credit card dimensions) and portable hand-held microsystem for biomolecular recognition applications based on a magnetoresistive biochip was developed. The microsystem integrates the magnetic biochip and all the electronic circuitry necessary for addressing, reading out, sensing, temperature controlling and fluid sample handling. Readout signals are processed through advanced signal processing techniques implemented in a digital signal processor (DSP). The DSP processes the recovered signals, reduces noise and offset effects, controls the biochip temperature and controls the analogue circuitry. High level system control and data analysis are remotely performed through a personal digital assistant via a wireless channel or a universal serial bus. A prototype has already been developed and experimental results show it may be used for magnetic label based bioassays [1].

The biochip (fabricated at INESC-MN using standard microfabrication techniques) has 256 biosensor detection sites (16×16). Each magnetoresistive sensor consists of a thin-film diode (TFD), $D_{i,j}$, connected in series with a MTJ, $S_{i,j}$, (fig. 1). Two different TFDs, Schottky (a-Si:H) and pin diodes, have been considered [4, 5]. Each TFD acts both as a switching device, enabling column, C_i, to row, R_j, connection, and as a temperature sensor of each biosensor site, $B_{i,j}$, [6, 1]. MTJs are very close to the TFDs and operate as a sensor of the planar magnetic field transversal to its length.

In the following a complete theoretical model describing biosensor electrical, temperature and magnetic behaviour is derived. Sensor modelling and characterisation is fundamental to sense local temperature, perform temperature control

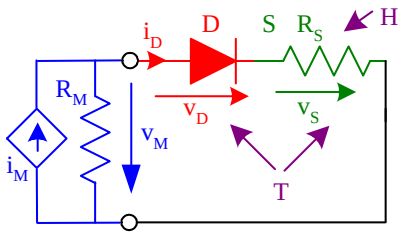

Figure 2: Biosensor element large signal model.

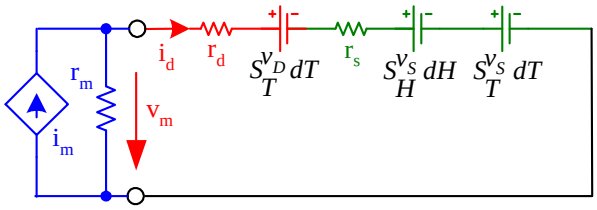

Figure 3: Biosensor element small signal model.

and achieve system calibration. In this paper *pin* diodes are specially considered as the switching and temperature sensing elements. Schottky diode modelling and characterisation specific aspects may be found in [5].

2. BIOSENSOR MODELLING

Considering the biosensor usage for DNA hybridisation detection, the site over each MTJ transducer is formerly functionalised with a DNA probe. The target DNA, tagged with paramagnetic nanoparticles, is transported in fluid and focused at sensing sites using alternating magnetic field gradients. Subsequently, DNA target hybridises with available complementary probe and finally, magnetic labels remain bound to the surface of the sensors after chip washing with a buffer solution.

An external magnetic field induces a magnetic moment on the nanospheres and each MTJ sensor will detect this change proportionally to the number of labels bound to its surface. The reading of each biosensor matrix element, $B_{i,j}$, is performed by a strategy of AC and DC current drive techniques in order to measure site temperature, T, and the local change, ΔH, of the external magnetic field, H, originated by the hybridisation of magnetically labelled DNA targets to the probes.

Each matrix element is driven with a measuring current source, i_M, and the small changes of the MTJs resistance are read as small voltage changes at the input driving port. Each biosensor element (TFD plus MTJ) may then be characterised by a large signal model (fig. 2) which takes into account the biosensor measured voltage, v_M, nonlinear relationship with the measuring current, i_M, absolute temperature, T, and external magnetic field, H, through the TFD and MTJ voltages (v_D and v_S, respectively):

$$v_M = v_D(i_M, T) + v_S(i_M, T, H) \qquad (1)$$

Since the current source usually has a very high internal resistance, the measuring current flows almost entirely through the biosensor, leading to $i_M \approx i_D$.

A small variation on each biosensor element voltage, $d\,v_M = v_m$, resulting from small changes or perturbations in the main variables, $d\,i_M = i_m$, $d\,T$ or $d\,H$, may be characterised through a small signal model (fig. 3), valid near a quiescent point (I_M, T, H):

$$d\,v_M = \underbrace{\frac{\partial v_D}{\partial i_M}}_{r_d} d\,i_M + \underbrace{\frac{\partial v_D}{\partial T}}_{S_T^{v_D}} d\,T + \\ + \underbrace{\frac{\partial v_S}{\partial i_M}}_{r_s} d\,i_M + \underbrace{\frac{\partial v_S}{\partial H}}_{S_H^{v_S}} d\,H + \underbrace{\frac{\partial v_S}{\partial T}}_{S_T^{v_S}} d\,T \qquad (2)$$

The different factors affecting all terms of dv_M are identified in the next sections through the *pin* diode and MTJ electrical, temperature and magnetic characterisation and modelling. It is shown that the diode has the ability to sense local temperature and the MTJ to act as the magnetic sensor.

3. *PIN* DIODE MODELLING

3.1. Diode Characterisation

Two different *pin* diodes (A and B) were experimentally characterised for a temperature range from room temperature until 85^oC and a voltage range between $-3\,V$ and $3\,V$. Temperature was set through a specially designed and built controller which allowed to stabilise the biochip temperature to a desired temperature target. Figures 4 and 5 show the diodes I-V characteristics. Because for low voltages diode characteristics present a negative current value, $|i|$ instead of i is depicted.

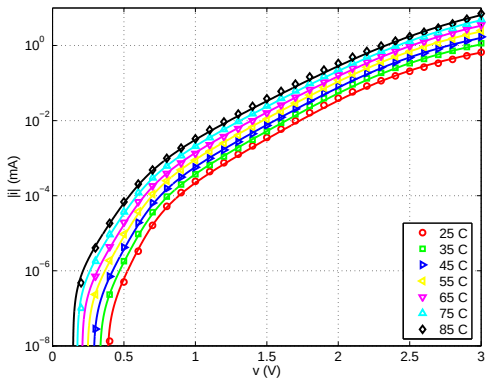

Figure 4: *pin* diode A — I-V characteristics: *a)* experimental data (marks); *b)* theoretically modelled characteristics (solid lines).

From the depicted data, three different regions may be considered: low, medium and high current values, each corresponding to a term contributing to the TFD v_D voltage (see

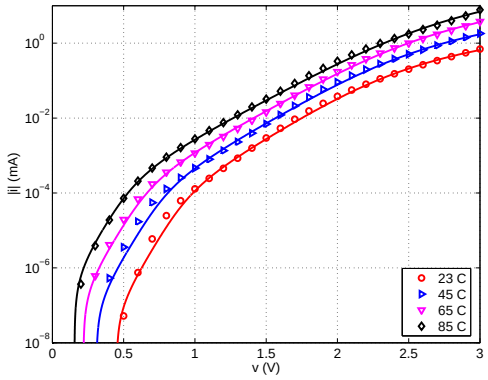

Figure 5: *pin* diode B — I-V characteristics: *a)* experimental data (marks); *b)* theoretically modelled characteristics (solid lines).

fig. 2 and eq. 1):

$$v_D = v_{J1} + v_{J2} + v_\alpha \tag{3}$$

In the following subsections a compound model is derived corresponding to these three different regions.

3.2. Diode at Low Currents

The low current region (LCR) is assumed to cover the $-0.5\,V$ to $0.5\,V$ voltage range. I-V characteristics for positive voltages show that a straight line approximation is possible but the characteristics do not pass through the origin. An offset is then considered, leading to a current I_0, the dark current, that may be modelled as a current source in parallel with the diode. The diode junction behaviour is then characterised by the Schockley equation [4] with I_0 included:

$$v_{J1} = n_1 V_T \ln\left(1 + \frac{i + I_0}{I_{S1}}\right) \tag{4}$$

where I_{S1} is the diode saturation current, n_1 is the emission coefficient, $V_T = K_B T/q$ is the thermal voltage and I_0 is the dark current value.

From experimental data and this theoretical model, semi empirical laws were derived for parameters dependence on temperature:

$$\log\left[I_{S1}(T)\right] = k_{11} - \frac{k_{21}}{T} \tag{5}$$

$$n_1(T) = n_{11} + n_{21} T \tag{6}$$

$$I_0(T) = \beta + (\gamma T)^\delta \tag{7}$$

For *pin* diode A equation parameters are: $k_{11} = 1.383\text{E}1$ and $k_{21} = 5.314\text{E}3$ for I_{S1} expressed in nA and T in K; $n_{11} = 9.477\text{E-}1$ and $n_{21} = 4.186\text{E-}3$; and $\beta = 7.207\text{E-}2$, $\gamma = 2.678\text{E-}3$ and $\delta = 1.758\text{E}1$ for I_0 also expressed in nA.

Marks in figure 6 show $I_{S1}(T)$, $I_0(T)$ and $n_1(T)$ estimated from the experimental data in the LCR. Yellow solid lines represent parameters modelling through the proposed laws. Figure 7 shows experimentally measured data (marks) for the LCR at several different temperatures and the modelled results with the LCR model. Although for the envisaged application only direct operation is of concern, it can be seen that both direct and reverse operation regions are very well characterised by the proposed LCR model. As expected, for voltage values above $0.5\,V$ the LCR model is inadequate and a medium current model must be derived.

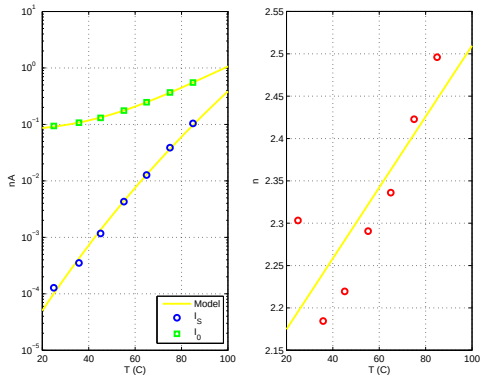

Figure 6: $I_{S1}(T)$, $I_0(T)$ and $n_1(T)$ characterisation and modelling: *a)* obtained from experimental data (marks); *b)* proposed model (solid lines).

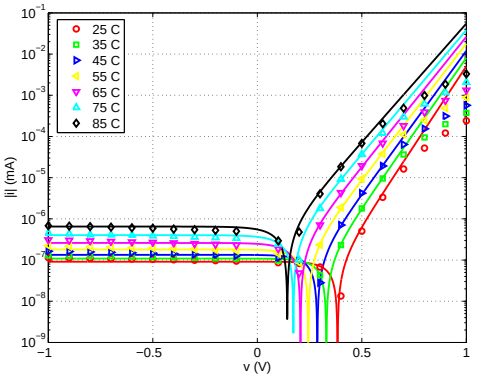

Figure 7: TFD I-V characteristic for the LCR: *a)* experimental data (marks); *b)* theoretically modelled (solid lines).

3.3. Diode at Medium Currents

For the medium current region (MCR), corresponding to TFD voltage values between $0.5\,V$ and $2\,V$, the Schockley equation is used to model the *pin* diode behaviour because its I-V characteristic suggests a typical diode response. The MCR model is:

$$v_{J2} = n_2 V_T \ln\left(1 + \frac{i}{I_{S2}}\right) \tag{8}$$

As for the LCR, model parameters dependence on temperature was derived and estimated values are shown in figure 8 as marks. Abnormally high values for the emission coefficient were obtained suggesting that, although the *pin* diode response in the MCR is being modelled as a single diode, its behaviour may correspond to the presence of more than one diode connected in series.

For the MCR model $I_{S2}(T)$ and $n_2(T)$ parameters dependence on temperature may be described by:

$$\log\left[I_{S2}(T)\right] = k_{12} - \frac{k_{22}}{T} \tag{9}$$

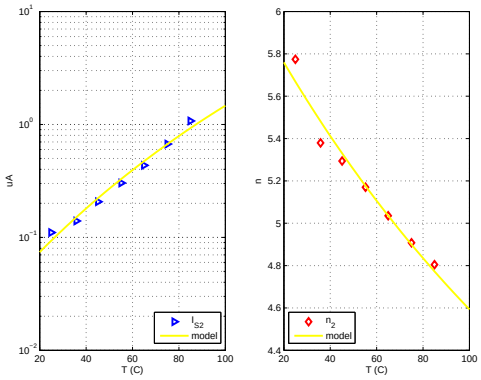

Figure 8: $I_{S2}(T)$ and $n_2(T)$ characterisation and modelling: *a)* obtained from experimental data (marks); *b)* proposed model (solid lines).

$$n_2(T) = n_{12} + \frac{n_{22}}{T} \tag{10}$$

Based on experimental data the following values were obtained for the parameter coefficients: $k_{12} = 7.921$, $k_{22} = 1.774\text{E}3$ for I_{S2} expressed in nA and T in K; and for the variation of the emission coefficient, $n_{12} = 3.179\text{E-}1$ and $n_{22} = 1.595\text{E}3$. Yellow solid lines in figure 8 show parameters temperature dependence modelling with the proposed laws.

Solid lines in figure 9 show TFD A response modelled with the LCR and MCR proposed models. An almost perfect match between the proposed model and experimental data until $2.25\,V$ is observed. From the point of view of the developed microsystem there is no need for an high current modelling because the maximum current allowed is limited by the magnetic junction. However, for the sake of completeness, a high current region model is now derived.

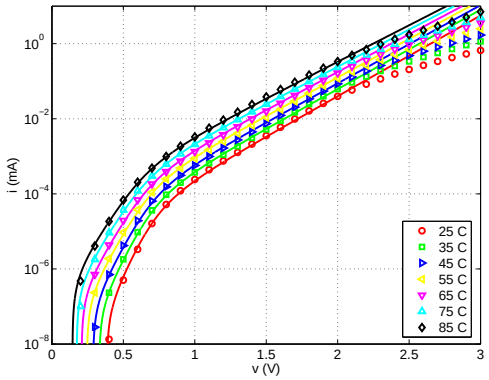

Figure 9: TFD I-V characteristic for the MCR: *a)* experimental data (marks); *b)* theoretically modelled (solid lines).

3.4. Diode at High Currents

The high current region (HCR), is defined for TFD voltage values from $2\,V$ to $3\,V$ and is modelled as a nonlinear resistive factor [5]:

$$v_\alpha = (Ri)^\alpha\,. \tag{11}$$

where both parameters have a temperature dependence that is modelled by:

$$\log\left[R(T)\right] = -r_1 + \frac{r_2}{T}, \tag{12}$$

$$\alpha(T) = \alpha_1 - \alpha_2 T, \tag{13}$$

For *pin* diode A extracted coefficient parameters are: $r_1 = 4.538$ and $r_2 = 2.180\text{E}3$ with R in Ω and T in K; and $\alpha_1 = 1.602$ and $\alpha_2 = 2.39736213\text{E-}3$. $R(T)$ and $\alpha(T)$ obtained from experimental data are depicted in figure 10 as marks and its modelling through the proposed laws is shown as solid yellow lines.

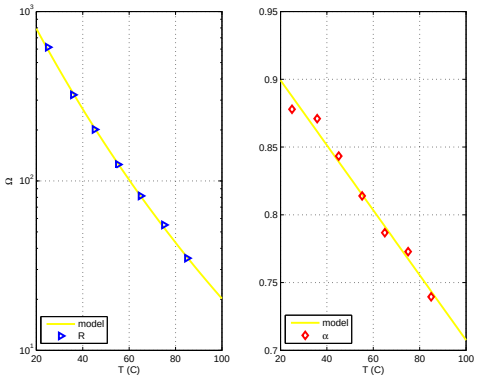

Figure 10: $R(T)$ and $\alpha(T)$ characterisation and modelling: *a)* obtained from experimental data (marks); *b)* proposed model (solid lines).

Figures 4 and 5, besides depicting the I-V experimental characterisation of the two, different, *pin* diodes A and B, also show the modelled characteristics (solid lines) obtained through the proposed models for the three current regions. It can be seen that the two diodes are very similar and the proposed compound model characterise both diodes over the entire voltage range.

3.5. Diode Dynamic Resistance

For the complete compound model the measured voltage sensitivity to the measuring current (eq. 2) is modelled by:

$$r_d = \frac{n_1 V_T}{i + I_0 + I_{S1}} + \frac{n_2 V_T}{i + I_{S2}} + \alpha R^\alpha i^{\alpha-1} \tag{14}$$

Figure 11 shows diode A $r_d(T)$ values calculated through eq. 14, both for room temperature and the maximum measured temperature. The corresponding experimental values, directly derived from experimental data are also shown as marks.

3.6. Diode Temperature Sensitivity

For the compound model the TFD voltage sensitivity to temperature (eq. 2) is:

$$S_T^{v_D} = S_T^{v_{J1}} + S_T^{v_{J2}} + S_T^{v_\alpha} \tag{15}$$

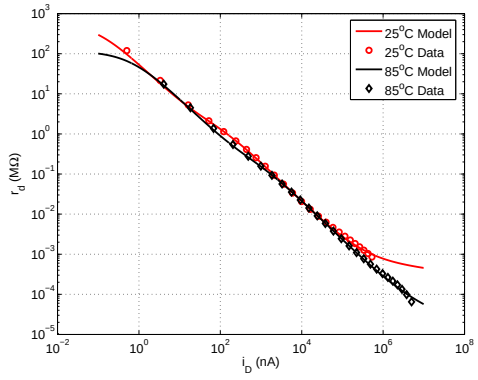

Figure 11: r_d for 25^oC and 85^oC: *a)* from experimental data (marks); *b)* from the proposed model (solid lines).

with:

$$S_T^{v_{J1}} = \frac{K_B}{q}\left[\frac{n_1\delta\,(\gamma T)^{\delta}}{i+I_0} - k_{21}\ln(10)\frac{n_1}{T} - \right.$$
$$\left. - (n_{11}+2n_{21}T)\ln\frac{I_{S1}}{i+I_0}\right] \quad (16)$$

$$S_T^{v_{J2}} = -\frac{K_B}{q}\left[n_{12}\ln\frac{I_{S2}}{i} + k_{22}\ln(10)\frac{n_2}{T}\right] \quad (17)$$

$$S_T^{v_\alpha} = -(Ri)^{\alpha}\left[r_2\ln(10)\frac{\alpha}{T^2} + \alpha_2\ln(Ri)\right] \quad (18)$$

Figure 12 shows, for several driving current values, the calculated sensitivities for *pin* diode A with the derived parameters. The complete compound model was considered and, for comparison purposes, results for the intermediate model for LCR and MCR are also depicted . The sensitivity variation with temperature does not show a perfect linear relation between the sensed voltage and the actual temperature value. In order to obtain accurate measures a calibration table, implemented on the onboard DSP, may be used to correct this nonlinear behaviour. Nonlinearity is more pronounced for very high current values, where the TFD is not expected to act as a temperature sensor.

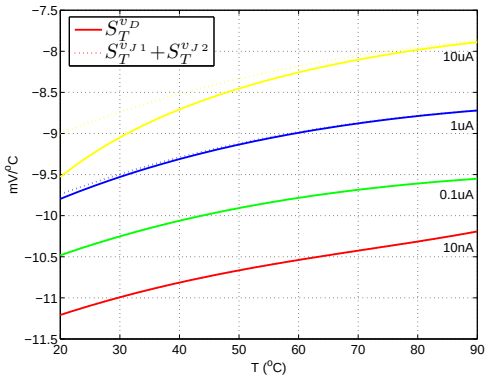

Figure 12: TFD voltage sensitivity to temperature: *a)* compound model (solid lines); *b)* LCR and MCR models only (dotted lines).

3.7. PIN Diode versus Schottky Diode

In a previous work a set of Schottky barrier diodes, with different characteristics, were considered [5]. *Pin* diodes reveal some advantages over Schottky diodes. First, their on/off ratio is higher, as shown in table 1, for applied voltages of $+2.5\,V$ and $-2.5\,V$. The on/off ratio is important because it limits biochip size. Both TFDs have the same dimensions, about $200\,\mu m \times 200\,\mu m$. This means that the *pin* diode current density is higher which allows to make smaller diodes for the same current value.

	Forward	Reverse	Ratio
Schottky	$6\times10^{-5}A$	$-0.4\times10^{-9}A$	1.3×10^{5}
pin	$2\times10^{-4}A$	$-1.2\times10^{-10}A$	1.6×10^{6}

Table 1: On/off ratios for *pin* and Schottky diodes

Pin diodes temperature sensitivity is also higher. For a driving current of $10\,nA$ Schottky diodes have about $-1.55mV/^oC$ sensitivity and *pin* diodes have about $-11mV/^oC$ sensitivity, although nonlinearity correction may be needed. Finally, it can be stated that *pin* diodes are also better behaved in the full current range, in the sense that they fit the proposed theoretical model more accurately, especially in the HCR. Besides, Schottky diodes do not present a such regular pattern on the I-V characteristics dependency on temperature as *pin* diodes do [5]

4. MTJ MODELLING

4.1 MTJ Electrical and Temperature Characterisation

The I-V characteristic of the biochips MTJs may be seen as having an almost linear characteristic. This is represented in fig. 13 where the I-V curves for three different temperatures are shown. The MTJ can be modelled by:

$$i = i_0 + R_0^{-1}v \quad (19)$$

Experimental data, as plotted in fig. 14, was used to determine the current and resistance variation with temperature, $R_0(T)$ and $i_0(T)$. Linear models were derived for their temperature dependence:

$$R_0 = R_x + \beta_x\,T, \qquad i_0 = i_x + \gamma_x\,T \quad (20)$$

A value of $\beta_x = -11.9\Omega/^oC$ was obtained. Solid lines in fig. 14 represent the behaviour predicted by these models. The match between predicted and experimental data show that the models can be used to characterise the biochip MTJs.

Typical MTJs may break down at applied voltages of over $1.1\,V$, limiting the maximum secure driving current at room temperature to approximately $70\,\mu A$ for a biochip with a nominal $R_0 = 15.3\,k\Omega$ (fig. 14).

For a drive current of $1\,\mu A$, a value of $S_T^{v_S} = -17.8\,\mu V/^oC$ was obtained. This is negligible when compared with $S_T^{v_D}$ exhibited by the TFD that is in series with it. It is then possible to use each biochip TFD as a temperature sensor and neglect the MTJ very low temperature sensitivity.

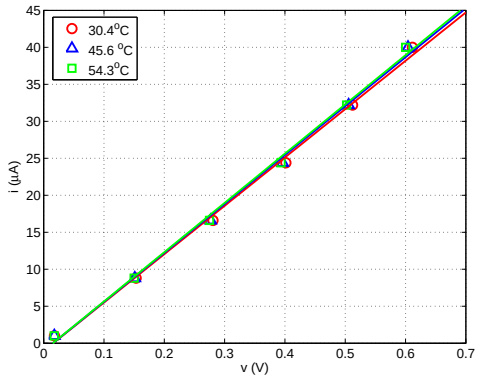

Figure 13: MTJ I-V characteristic at different temperatures.

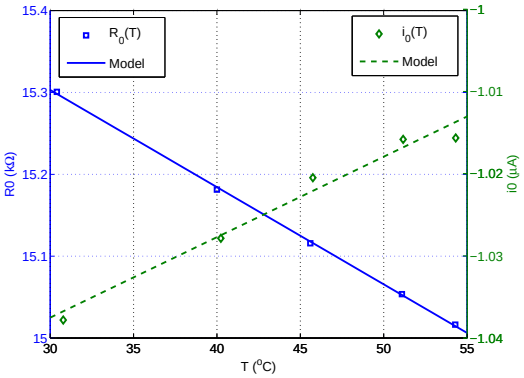

Figure 14: MTJ $R_0(T)$ and $i_0(T)$ and corresponding models characteristics.

4.2 MTJ Magnetic Characterisation

MTJ resistance varies with the transversal component of an applied magnetic field and its sensitivity is measured by the tunnelling magnetoresistance ratio, *TMR*.

$$TMR = \frac{R_{\max} - R_{\min}}{R_{\min}} \times 100\,\% \qquad (21)$$

where R_{max} and R_{min} are the maximum and minimum resistance values obtained with magnetic opposite saturation fields (typically ± 10 Oe, ΔH_{max}). The TMR decreases with the applied voltage, being maximum for zero applied voltage and almost constant until 30 mV ($TMR(0) \cong 27\%$ was obtained) and then decreases almost linearly with bias voltage increase (fig. 15). In the range $300 - 500mV$ (where TMR drops to half its initial value) it is possible to model:

$$\frac{TMR(V)}{TMR(0)} = 1 - \frac{V}{2V_{1/2}} \qquad (22)$$

showing MTJ *TMR* dependence on the applied DC bias voltage. However, a bias voltage reduction implies a driving current reduction, reducing the reading voltage, v_M (fig. 3). Driving current optimization is then needed in order to maximize v_M. Its value may be derived taking into account that:

$$S_H^{v_S} = S_H^{R_S} \times i_M, \qquad S_H^{R_S} = TMR(V)\frac{R_S}{\Delta H_{\max}} \qquad (23)$$

Its value may be estimated as $V_{1/2}/R_S$. Experimental characterisation of one of the biochip MTJs showed a resistance of $14.4k\Omega$ and ΔV_{max} occuring for a drive current of approximately $30\,\mu$A.

Increasing MTJ resistance decreases the current required to maximize signal output but at the expense of increased sensor noise (mostly $1/f$ for low frequency applications). Lowering MTJ resistance pushes the maximum signal peak to higher currents.

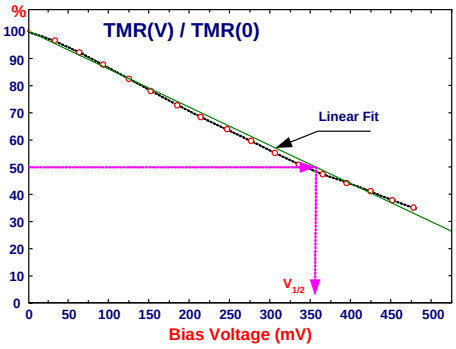

Figure 15: MTJ dependence on bias voltage.

5. CONCLUSION

A magnetoresistive biosensor for biomolecular recognition has been characterised and modelled. Biosensor sites consisting of a series of a *pin* thin-film diode and a magnetic tunnel junction were analysed from the point of view of their electrical, temperature and magnetic properties. Theoretical proposed models may be used for biochip characterisation and calibration. Experimental results show that the TFD may be effectively used as a switching device and a temperature sensor and that the MTJ characteristics allow its usage as the magnetic sensing element for the envisaged biochip application.

References

[1] J. Germano *et al.* Microsystem for Biological Analysis based on Magnetoresistive Sensing. In *Proc. of the XVIII IMEKO World Congress*, 2006. (Sep. 17-22).

[2] W. Shen *et al.* In situ detection of single micron-sized magnetic beads using magnetic tunnel junction sensors. *Appl. Phys. Lett.*, 86(253901), 2005.

[3] H. A. Ferreira *et al.* Biodetection using magnetically labelled biomolecules and arrays of spin valve sensors. *Journal of Applied Physics*, 94(10):1–5, 2003.

[4] S. M. Sze. *Physics of Semiconductor Devices*. John Wiley & Sons, 2 edition, 1981.

[5] T. M. Almeida *et al.* Microsystem for Biological Analysis based on Magnetoresistive Sensing. In *Proc. of the 2006 IEEE Instrumentation and Mesurement Technology Conference*, 2006. (Apr. 24-27).

[6] M. Piedade *et al.* Architecture of a Portable System Based on a Biochip for DNA Recognition. In *Proc. of the XX Conference on Design of Circuits and Integrated Systems*, 2005. (Nov. 23-25).